molecular pharmaceutics

Article

pubs.acs.org/molecularpharmaceutics

In Vivo Distribution and Toxicity of PAMAM Dendrimers in the Central Nervous System Depend on Their Surface Chemistry

Lorenzo Albertazzi,*[,†,‡] Lisa Gherardini,[§,∥] Marco Brondi,[†,‡] Sebastian Sulis Sato,[†,‡] Angelo Bifone,[†] Tommaso Pizzorusso,[§,#] Gian Michele Ratto,[‡,⊥] and Giuseppe Bardi*[,†]

[†]Center for Nanotechnology Innovation @NEST, Istituto Italiano di Tecnologia, Piazza San Silvestro 12, 56127 Pisa, Italy

[‡]Laboratorio NEST, Scuola Normale Superiore, Piazza San Silvestro 12, 56127 Pisa, Italy

[§]Institute of Neuroscience—CNR, Via Moruzzi 1, 56124 Pisa, Italy

[∥]Institute of Clinical Physiology—CNR, Via Fiorentina 1, 53100 Siena, Italy

[⊥]Institute of Nanoscience—CNR, Via di San Niccolò, 89a-95 50125 Florence, Italy

[#]Department of Psychology, University of Florence, Via di San Niccolò, 89a-95 50125 Florence, Italy

Supporting Information

ABSTRACT: Dendrimers have been described as one of the most tunable and therefore potentially applicable nanoparticles both for diagnostics and therapy. Recently, in order to realize drug delivery agents, most of the effort has been dedicated to the development of dendrimers that could internalize into the cells and target specific intracellular compartments in vitro and in vivo. Here, we describe cell internalization properties and diffusion of G4 and G4-C12 modified PAMAM dendrimers in primary neuronal cultures and in the CNS of live animals. Confocal imaging on primary neurons reveals that dendrimers are able to cross the cell membrane and reach intracellular localization following endocytosis. Moreover, functionalization of PAMAMs has a dramatic effect on their ability to diffuse in the CNS tissue in vivo and penetrate living neurons as shown by intraparenchymal or intraventricular injections. 100 nM G4-C12 PAMAM dendrimer already induces dramatic apoptotic cell death of neurons in vitro. On the contrary, G4 PAMAM does not induce apoptotic cell death of neural cells in the sub-micromolar range of concentration and induces low microglia activation in brain tissue after a week. Our detailed description of dendrimer distribution patterns in the CNS will facilitate the design of tailored nanomaterials in light of future clinical applications.

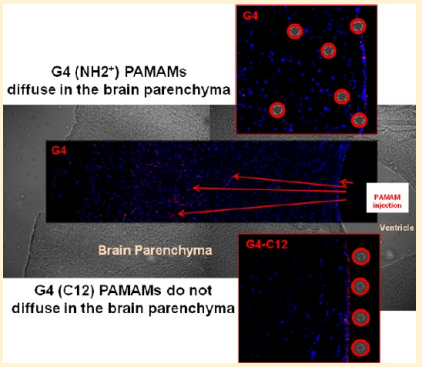

KEYWORDS: *dendrimers, neurotoxicity, nanomaterials, neurons, central nervous system*

INTRODUCTION

Dendrimers are very promising nanomaterials for therapeutic and diagnostic purposes.[1] Because of their unique tree-like structure they are endowed with many desirable properties. In particular, their monodispersity and tunable properties make dendrimers very attractive for biomedical applications.

The commercially available polyamidoamine (PAMAM) dendrimers could be easily functionalized changing their properties such as surface charge or lipophilicity, enhancing their wide use for a range of biological applications such as drug or gene delivery, biosensing and contrast agents.[2] Although widespread applications of PAMAMs in vitro have been reported[3] many aspects of their behavior in vivo are still to be unveiled. We and other groups recently report that structural features such as charge, size and hydrophobicity drive dendrimer interaction with cells and tissues and in particular their trafficking in living cells.[4−6] However, although characterization of dendrimers with cell cultures is a fundamental step to reveal crucial features, specific clinical applications need more reliable and representative models.

One of the most ambitious challenges of drug delivery is the treatment of central nervous system (CNS) diseases as most of the drugs and employed nanoparticle carriers do not cross the blood−brain barrier (BBB). Moreover particle diffusion in the brain tissue and toxicity are still main issues. In the present work, we used confocal and two-photon microscopy analysis to identify the biological properties of specifically functionalized PAMAM dendrimers into primary neuronal cultures and CNS in vivo. In particular we focused our attention on two specific issues: (i) the ability of functional PAMAM dendrimers to diffuse in the brain tissue and be subsequently internalized in neurons; (ii) a detailed study of toxicity of PAMAM in the CNS.

To reach the CNS parenchyma it is essential to assess the most suitable delivery methods.[7−9] To deliver dendrimers to the CNS we employed three different methods, namely, intraparenchymal,

Received: July 18, 2012
Revised: November 15, 2012
Accepted: November 19, 2012

   dx.doi.org/10.1021/mp300391v | *Mol. Pharmaceutics* XXXX, XXX, XXX−XXX

intraventricular and subarachnoid injections. Each of these methods overcomes the crossing of the BBB, resulting in minimally invasive procedures already used for experimental[10] and clinical applications.[11−13] Nevertheless, our detailed study of dendrimer diffusion and internalization ability in the brain tissue by the mentioned methods of delivery offers important information for studying nanoparticles aimed at the BBB crossing.

These imaging techniques revealed the ability of dendrimers to cross cell membranes allowing the identification of intracellular endocytosis pathways. Different PAMAM dendrimer surface functionalization resulted in dramatic effects on their ability to diffuse in brain parenchyma and neural cell internalization. In light of future clinical applications, we described dendrimer toxicity profile evaluating neuron cell death and activation of CNS resident immune system, namely microglia, upon PAMAM dendrimer injections. Our observations will help the design of tailored nanomaterials for drug or gene delivery aimed at CNS diseases.

EXPERIMENTAL SECTION

Dendrimers. PAMAM (ethylenediamine core, generation 4.0; Cat. No. 412449) and PAMAM-25% C12 (ethylenediamine core, generation 4; Cat. No. 536962) 10% w/w methanol solutions were purchased by Sigma-Aldrich Ltd. Dendrimers were labeled and characterized as previously reported.[14] Briefly, PAMAM dendrimers were conjugated with Alexa 647 fluorophore to prepare infrared-labeled PAMAM dendrimers. Conjugation has been carried out via amide bond between the primary amine of the dendrimer and the *N*-hydroxysuccinimide activated carboxyl of the fluorophores. Dendrimers (50 nmol) were dissolved in carbonate buffer at pH 9 and mixed with a DMSO solution of reactive dye (2 equiv for dendrimer). Three net negative charges (Alexa 647) have been added per 2 amine groups of the dendrimers. Labeling of dendrimer surface resulted in 58 $-NH_2$ groups on Alexa 647-modified G4 PAMAM vs 64 $-NH_2$ groups on commercial G4 PAMAM; and 42 $-NH_2$ on Alexa 647-modified G4-C12 PAMAM instead 48 $-NH_2$ on G4-C12 PAMAM. The solution was stirred for 4 h at room temperature and then dialyzed against water (MWCO = 10 kDa) to afford dendrimer−dye conjugates. Owing to the poor solubility of lipid modified dendrimer PAMAM (25% of surface lipid groups) basic aqueous solutions, the reaction was carried out in DMSO (4 h at room temperature) and then dialyzed against water.

Primary Neural Cell Cultures. Primary mouse cortical cultures were prepared as previously reported.[15] Briefly: brains were removed from mice at postnatal days 0−2 and placed in HBSS. Cortices were dissected and meninges removed. Chopped small pieces of cortex were triturated with a Pasteur pipet in the presence of 0.25% trypsin and DNAse to reach a single-cell suspension. After 5−10 min a small volume of suspension at the top was placed in an equal volume of DMEM supplemented with 10% horse serum. Cells were then counted and directly cultured on coverslips or Petri dishes previously coated with 100 mg/mL polylysine. After 2 h DMEM/horse serum was replaced with Neurobasal-A medium supplemented with 1% B27, 2 mM glutamine and gentamicine. After 7 days fully differentiated neurons lay on glia cells growing in a layer underneath the neurons.

Apoptosis Assays and in Vitro Microscopy. Fluorescence and phase contrast pictures of primary cortical cultures were taken without or with increasing concentrations of G4 PAMAM and G4-C12 PAMAM (1 to 100 nM). 0.5 Hoechst 33258 nuclei staining, 5 nM DiO-C6 (Sigma-Aldrich, St. Louis, MO, USA) membrane staining (30 min, RT, dark) and phase contrast cell morphology were used to evaluate differences between normal and apoptotic cells after treatments. Normal cell morphology was considered as "viable cell" whereas apoptotic cell presented picnotic nuclei and membrane blebbing. This morphology allowed us to discriminate between viable and apoptotic cells in the different samples tested. Phase contrast and fluorescence cell images were acquired by a camera mounted Zeiss Axioskop microscope and by Leica SP2 confocal microscope. A least three independent experiments have been performed, and one-way analysis of variance (ANOVA) followed by Newman−Keuls multiple comparison tests has been used for statistic evaluation of the results.

Animals. All procedures were performed according to the guidelines of the Italian Ministry of Health for care and maintenance of laboratory animals (law 116/92) and in strict compliance with the European Communities Council Directive 86/609/EEC.

Intracerebroventricular Injection. 10 μM solutions of G4 and G4-C12 in PBS were injected individually into the mouse cerebroventricles. The scull of anesthetized animals mounted on a stereotaxic apparatus was exposed. A single aperture at stereotaxic coordinate (−0.50 mm M-L; 1.0 mm A-P from Bregma, Paxinos adult mouse brain Atlas) was manually obtained by gently pressing the surface of the scull using a smooth tip needle protected by a silicon mask only to expose 3 mm length of free metal surface. A Hamilton precision syringe was used to slowly (0.5 μL/min) inject 2 μL of dendrimer solution into the third ventricle. The scalp was then sutured and the animals were laid to recover until sacrificed 6 h later and intracordially perfused with 4% paraformaldehyde

Intraparenchyma Injection. Anesthetized mice were placed on a stereotactic platform, and the scalp was incised to expose the cranium. A small hole was drilled in the skull bilaterally above the primary motor cortex (M1, +0.5 mm and +1.5 mm from Bregma). 1 μL of G4 dendrimer solution was stereotaxically injected into the cortical parenchyma of the left hemisphere. The G4 dendrimer solution was manually delivered via a glass micropipet connected to a syringe at a depth of 0.700 mm from the brain surface at its injection site at a rate of 0.5 μL/min with a 1 min interval before retraction of the micropipet from the tissue. As internal positive control 1 μL of solution of lipopolysaccharides (LPS 3 μg/μL; *Salmonella abortus equii*, Sigma-Aldrich, St. Louis, MO) was injected in the contralateral M1 cortex. Animals were sacrificed 10 days after treatment and perfused with a solution of 4% paraformaldehyde.

Immunostaining. Brain tissue was kept in 4% paraformaldehyde overnight, cryoprotected in 30% w/v sucrose solution for at least 48 h and snap-frozen at −40 °C (isopentane solution on dry ice). The specimens were then sectioned with a cryostat at −20 °C to obtain 60 μm thick sections. Slices were recovered in a well plate in PBS and preserved at 4 °C until further analysis. To image cell nuclei in the tissue, a nuclear staining was performed by simply submerging the selected sections into a 1:10 diluted solution of Hoechst 33342 nuclear stain (0.5 mg/mL, Sigma) in PBS for 10 min. Slices were then washed with PBS and mounted on microscope glasses and covered with VectaShield mounting medium (Vector Laboratories, Burlingame, CA) to prevent fluorescence fading. Activation of microglia was achieved using LPS (see preceding paragraph) and evaluated using IBA1 monoclonal staining, and free-floating sections were blocked in

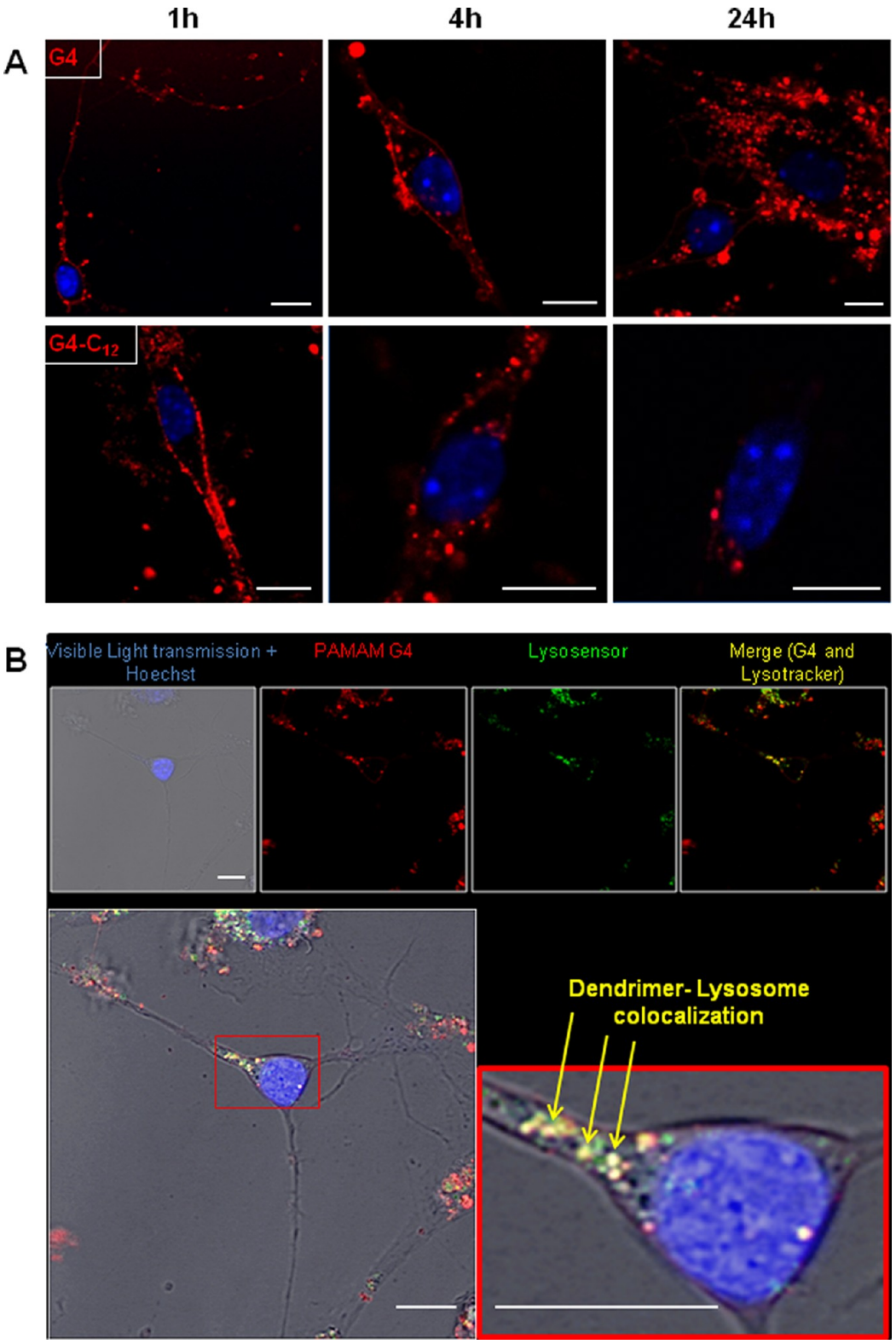

Figure 1. (A) Time lapse imaging of intracellular localization of G4 and G4-C12 in primary neuronal cultures. 10 nM dendrimer (in red) localization after 1 h, 4 h and 24 h after administration. Nuclei are stained in blue with Hoechst. (B) Colocalization assay of G4 dendrimer using LysoTracker in primary neurons. Overlay of transmission and fluorescence images (Hoechst 33258, blue; AF647 labeled dendrimer, red; LysoTracker, green). Scale bar = 10 μm.

10% BSA, 0.3% Triton X-100 in PBS for 2 h at room temperature, then incubated overnight at room temperature in a PBS solution with 1% BSA, 0.1% Triton X-100, and 1:500 polyclonal rabbit IBA1 primary antibody and a monoclonal 1:500 anti-GFAP primary antibody (Synaptic Systems). The signals were detected by incubation in 1% BSA, 0.1% Triton X-100, and 1:400 goat anti-mouse secondary antibody conjugated to Alexa Fluor-488 fluorophore (to detect microglia) and 1:400 goat anti-rabbit

dx.doi.org/10.1021/mp300391v | *Mol. Pharmaceutics* XXXX, XXX, XXX–XXX

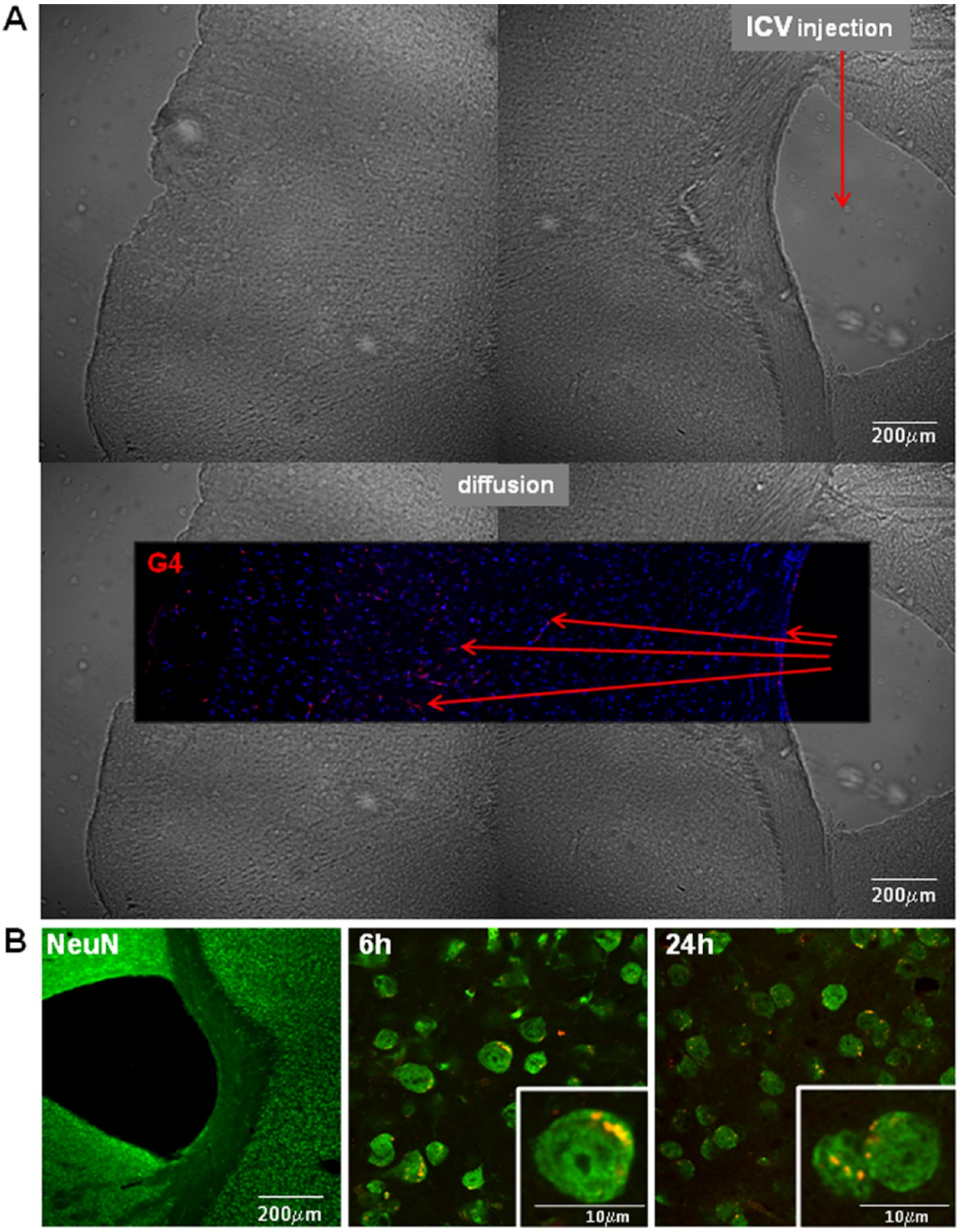

Figure 2. G4 PAMAM dendrimer crossing of ependymal barrier and diffusion into the parenchyma. (A) Confocal images in transmission light of brain tissue after ICV injection. In the central overlaid fluorescence image, nuclei were stained with Hoechst 33258 (blue) and G4 PAMAM labeled with AF647 (red). (B) Specific neuron staining NeuN (green) after ICV injections of G4 dendrimers (red). Low magnification image of NeuN staining around the cerebral ventricle (left) and high resolution colocalization with G4 PAMAM after 6 h (middle) and 24 h (right).

secondary antibody conjugated to Alexa Fluor-563 fluorophore (astrocyte signal) (Molecular Probes, Eugene, OR) for 2.5 h at room temperature. Sections were mounted on glass slides using VectaShield mounting medium. This staining was applied at specimens from intraparenchyma injection.

TUNEL Staining for Apoptosis Detection in Vivo. To detect apoptosis in vivo we used ApoAlert DNA Fragmentation Assay Kit (Clonetech Laboratories, Inc., Mountain View, CA, USA), a fluorescence kit based on terminal deoxynucleotidyl transferase (TdT)-mediated dUTp nick-end labeling (TUNEL). Briefly, free-floating paraformaldehyde fixed 50 μm coronal sections were treated for 5 min at room temperature (RT) with 20 μg/mL Proteinase K solution. After washing with phosphate buffered saline (PBS) solution (0.1 M) the slices were

dx.doi.org/10.1021/mp300391v | *Mol. Pharmaceutics* XXXX, XXX, XXX−XXX

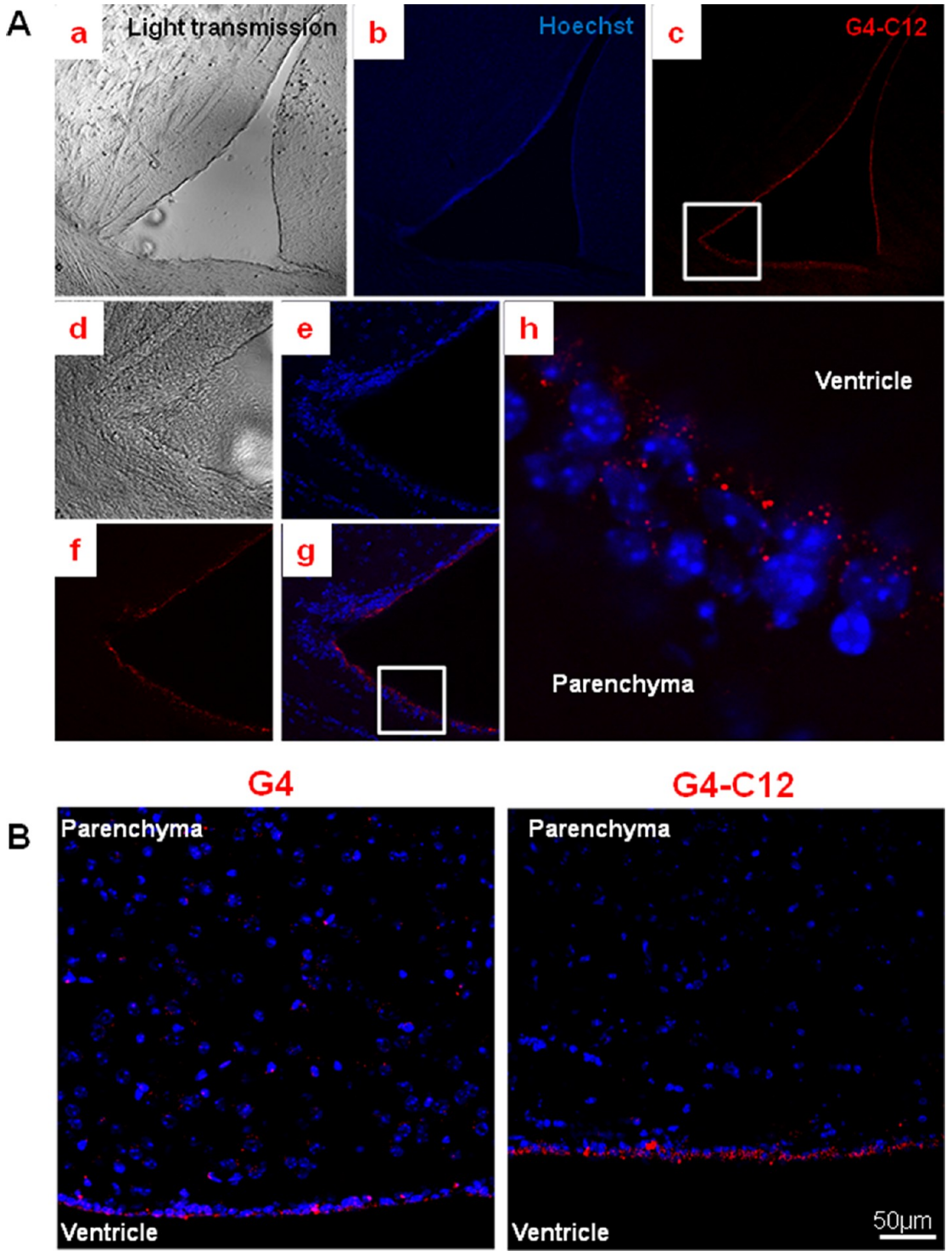

Figure 3. G4-C12 PAMAM dendrimer does not cross the ependymal barrier. (A) An entire ventricle is shown in visible light transmission (a) and Hoechst 33258 staining (b).The accumulation of the G4-C12 lipophilic dendrimer in the ependymal cell layer is visible in red (c). In panels d, e and f a detail of the ependymal border is highlighted by cell nuclei (Hoescht 33258) and dendrimers (red). Panel g represents the fluorescence overlay, and panel h represents G4-C12 dendrimer surrounding the ependymal cell nuclei (blue). (B) The two images confront G4 diffusion dendrimers within the brain parenchima and G4-C12 localization within the ependymal layer on the boundary of the ventricle.

equilibrated with equilibration buffer at RT for 10 min. TdT incubation buffer was prepared following the Kit User Manual suggested ratios of equilibration buffer, nucleotide mix, and TdT enzyme. The tailing reaction was performed in the dark and humidified 37 °C incubator for 60 min. The reaction was terminated by adding 2× SSC and incubating for 15 min at RT in the dark. The slices were washed with PBS before mounting on microscope slides. Slices were mounted on glass slides with VectaShield (H1000; Vector Laboratories), and preparations were coverslipped and sealed with nail polish before imaging.

Confocal Imaging. Slice imaging was performed on a Leica TCS SP2 inverted confocal microscope (Leica Microsystems)

dx.doi.org/10.1021/mp300391v | *Mol. Pharmaceutics* XXXX, XXX, XXX−XXX

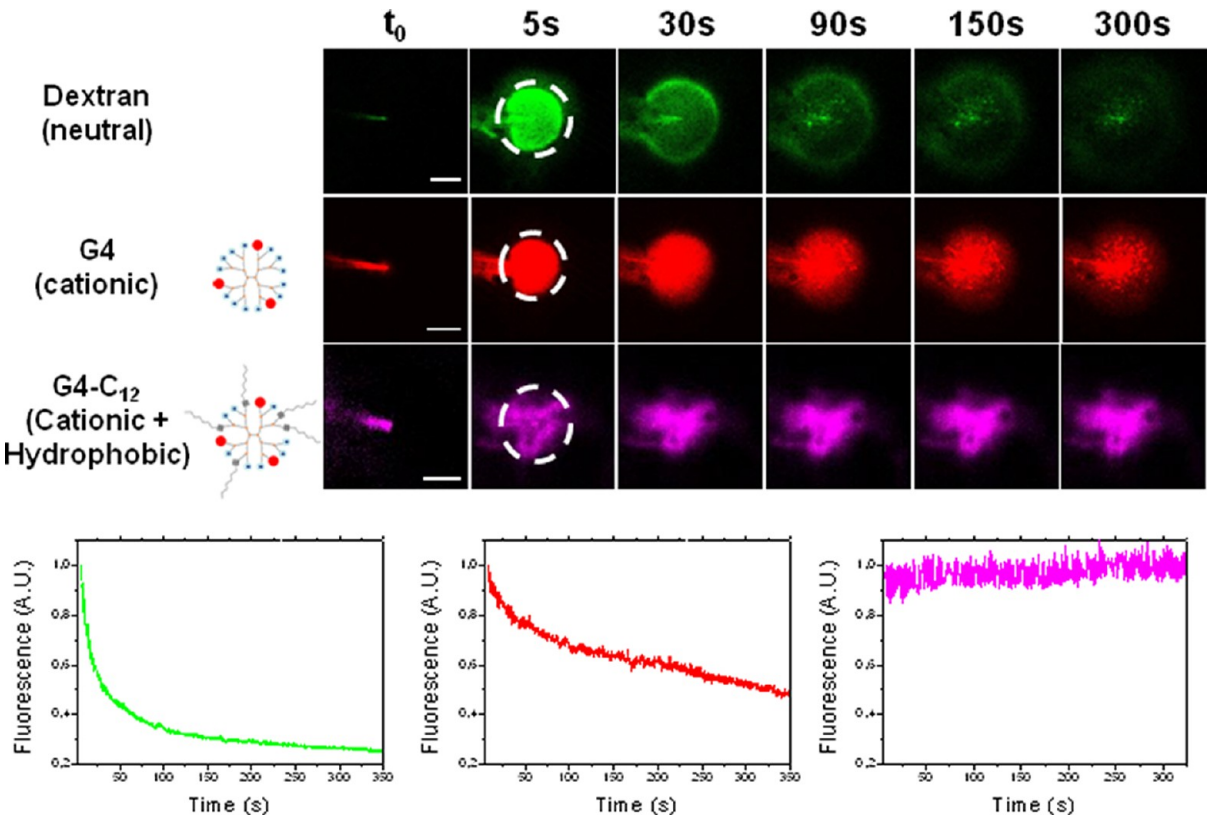

Figure 4. Two-photon in vivo imaging of dendrimer diffusion in brain. Time lapse of G4 (red) and G4-C12 (purple) dendrimer injections in the brain cortex of living mice. In t_0 images the tip of the pipet could be observed. Dendrimers were injected for 5 s, and then fluorescence in the injection site was measured. Dextran (green) was used as control. The time evolution of the fluorescence signal in the injection site is reported (bottom). Scale bar = 100 μm.

equipped with a 40× 1.25 NA oil immersion objective (Leica Microsystems). Imaging was obtained illuminating the samples with the inline Ar and He−Ne lasers of the microscope and with a 403 nm pulsed diode laser (M8903-01; Hamamatsu) at 50 MHz repetition rate. Fluorescence emission was collected with the AOBS-based built-in detectors of our confocal microscope (Hamamatsu R6357).

2-Photon Imaging. Experiments were performed at 3−4 weeks of age on C57/BL6-j mice. Mice were anesthetized with urethane (1.6 gr/kg) and ventilated with O_2 enriched air; a unilateral craniotomy above the visual cortex (centered 2 mm from the midline) was opened and the cortex surface constantly kept superfused with artificial cerebrospinal fluid (ACSF). A glass pipet was employed to inject in the cortex (150 μm depth, tip diameter 2 μm, pressure of 0.5 psi) the dendrimer. In vivo two-photon imaging was performed with an Ultima Multiphoton Microscopy System (Prairie Technologies) equipped with a Mira 900 mode-locked laser source (Coherent). Dyes were excited with 820 nm radiation, and their emission was collected through bandpass filters. Excitation laser power was adjusted to minimize photobleaching.

RESULTS

Confocal Imaging of PAMAMs Dendrimers in Primary Cortical Neurons. Interactions of amine-terminated and mixed amine-C12 aliphatic chain generation 4 (G4) dendrimers with primary neurons were evaluated. These two structures were chosen as they showed the best ratio between cell internalization and toxicity in different cell lines.[14] Dendrimers were labeled with the infrared Alexa 647 in order to follow their localization by confocal microscopy.

Time lapse imaging of neurons after administration of dendrimers was performed, and the results are reported in Figure 1A. One hour after 10 nM G4 dendrimer administration, neurons presented strong fluorescence signal from the plasma membrane indicating high affinity of the cationic materials for the negatively charged cell surface. Little internalization occurred in this time period, and most of the signal was localized on the cell membrane. At a later stage (4 h) vesicles moving toward the nucleus were observed, although weak membrane localization was still present. Eventually, after 24 h most of the G4 and G4-C12 PAMAMs was placed in the perinuclear region. Figure 1B shows G4 detected with LysoTracker 24 h after administration (G4-C12 lysosome colocalization was also observed 4 h after administration, as represented in Figure 1 in the Supporting Information). The high colocalization degree indicates that lysosomal vesicle compartment is the final fate of PAMAMs trafficking in neurons. These results are in agreement with our previous observation in cell lines,[14] however, the slower internalization observed here correlates with the slower membrane recycling rate of primary neurons. This event highlights the ability of cationic PAMAMs to be internalized by endocytosis in primary neurons and to be delivered to the lysosome.

Distribution of PAMAM Dendrimers into the Brain Parenchyma in Vivo. We employed confocal microscopy to describe the local cellular compartmental distribution as well as the middle- to long-term dendrimer pattern of diffusion into the

dx.doi.org/10.1021/mp300391v | *Mol. Pharmaceutics* XXXX, XXX, XXX−XXX

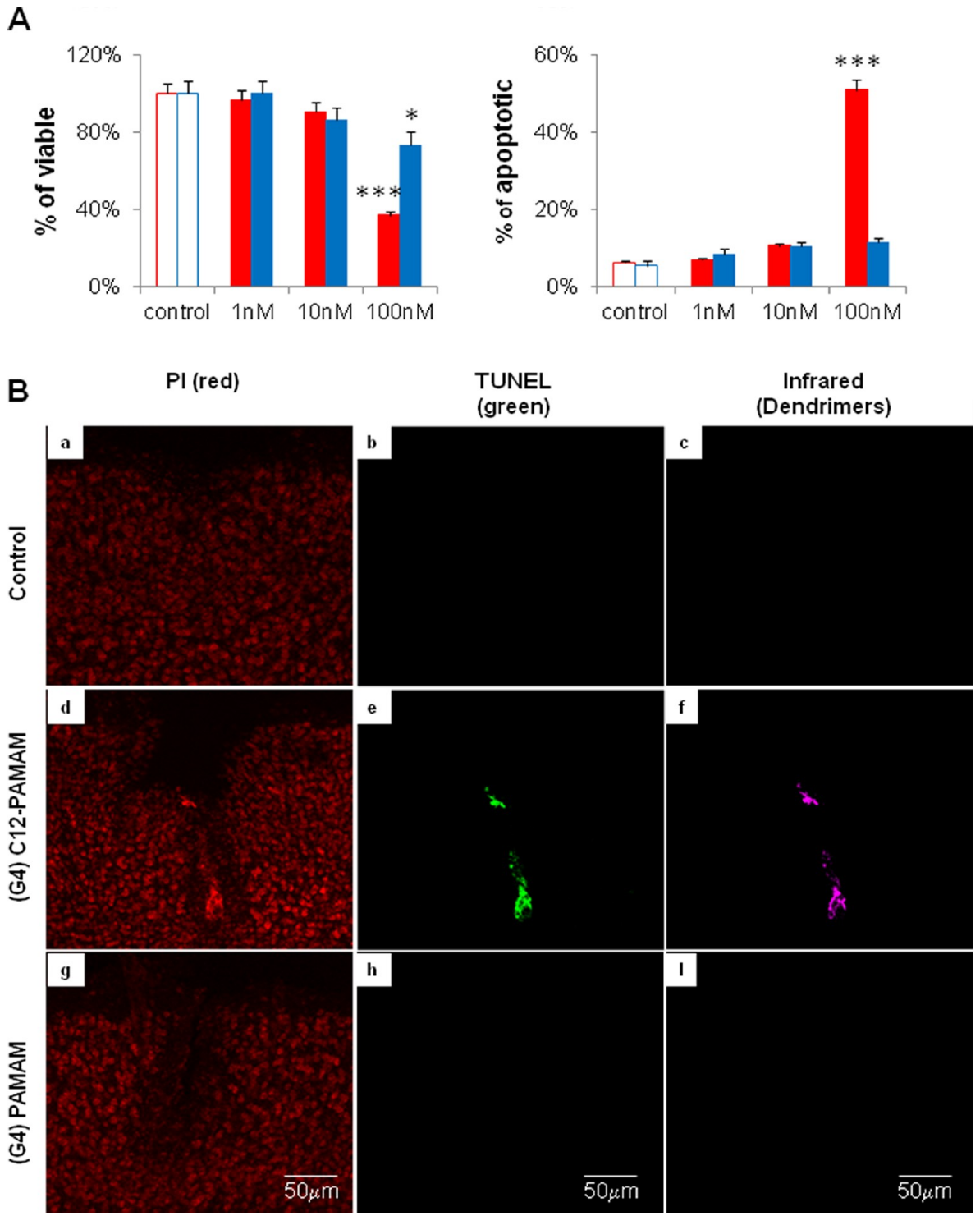

Figure 5. G4-C12 PAMAM dendrimer induces apoptosis in primary cortical neuron in vitro and in vivo. (A, left graph) Viable neurons were counted 24 h after treatment with step-increasing concentration of G4 (blue bars) and G4-C12 (red bars) PAMAM dendrimers, and the results were expressed in percentage of remaining cells after treatments compared to control (untreated). Quantification of apoptotic neurons measured by picnotic nuclei (Hoechst staining) and membrane blebbing (DIO-C6 staining) are shown in the bar graph on the right. The data are expressed as mean ± SEM of three independent experiments. One-way analysis of variance (ANOVA) followed by Newman−Keuls multiple comparison tests (treatments vs control, $*P < 0.05$; $**P < 0.01$; $***P < 0.001$) was performed. (B) Confocal microscopy pictures of stained mouse brain coronal sections are presented after G4 and G4-C12 PAMAM dendrimer intracortical injections. In panels a, d and g pictures show propidium iodide staining (red) of the brain cortical cell nuclei to reveal the damage at the injection site. Panels b, e and h represent the signal at 520 nm emission wavelength for apoptotic cell detection by TUNEL assay (apoptotic cells become FITC stained, green emitting fluorescence). Panels c, f and i report infrared-labeled dendrimer fluorescence imaging of the same area.

brain parenchyma in vivo which provides crucial information for the development of dendrimer-based brain delivery systems.

Intraventricular (ICV) injections (Figure 2) of 10 μM Alexa 647 labeled G4 and G4-C12 PAMAM solutions were performed

dx.doi.org/10.1021/mp300391v | *Mol. Pharmaceutics* XXXX, XXX, XXX−XXX

in anesthetized mice. Such high dendrimer concentration is justified by the further dilution in the roughly 4−5 mm^3 volume of the mouse CSF.[16] This experiment explicates the possibility of dendrimers to cross the ventricle barriers and penetrate into the brain tissue in view of delivery applications. Animals were sacrificed 24 h after ICV injection. Hoechst stained brain tissue slices (Figure 2 in the Supporting Information) were imaged with confocal microscopy. Amino G4 dendrimers freely diffuse in the cerebrospinal fluid and cross the ependymal cell border penetrating the brain parenchyma (Figure 2A). Alexa 647 fluorescence revealed G4 PAMAM localization up to the outer cortical layers (central fluorescence image).

Co-staining of brain tissue with specific neuronal nuclear staining NeuN (Figure 2B) emphasizes G4 PAMAM dendrimer localization in neurons, progressing in time with prolonged incubation (6 h and 24 h). The nuclear staining of neurons highlights perinuclear localization of the dendrimer, very similar to what is observed in vitro, and suggests endolysosomal accumulation.

On the contrary, the majority of the G4-C12 dendrimers is retained in the proximity of the ependymal stratum when injected into the ventricle, and no signal is detectable within the brain parenchyma (Figure 3Ac). High magnification images (Figure 3Ad−h) show an accumulation of dendrimers lining the ventricles within the ependymal cell layer.

Figure 3B highlights how the C12 lipid moieties on the dendrimer can affect PAMAM accumulation on the ependymal barrier (right panel) in contrast to the amine-functionalized G4 (left panel), which is able to cross the barrier and distribute into the brain parenchyma.

Moreover, in order to understand whether parenchyma penetration of G4 PAMAM from the CSF was not limited to the ventricle sites, we performed subarachnoid injection of the dendrimer solution. As expected, G4 PAMAM dendrimers managed to escape the ependyma and diffuse throughout the layers up to the CNS dural surface (Figure 3 in the Supporting Information). These findings suggest that G4 holds promising features for the developing delivery system aimed at deeper brain parenchyma sites.

Two-Photon Study of Dendrimer Diffusion in Vivo. To investigate the diffusion kinetics of PAMAMs into the brain parenchyma we performed 2P-microscopy in living animals after direct intraparenchymal (IP) injection (Figure 2 in the Supporting Information). This technique provides a clear-cut analysis of the immediate distribution behavior of both G4 and G4-C12 dendrimers. This is a crucial and rather unexplored feature to developing nanocarriers.

Figure 4 shows the 2-photon (2P) imaging of the injections of G4 and G4-C12 in the brain cortex. Dendrimers were injected for 5 s from a glass pipet (4 μm tip) at 150 μm depth into the brain cortex under 2P imaging after while the fluorescence in the injection site was measured upon time. As clearly shown, a dramatic effect of the different surface functionalization was observed. In fact, G4 dendrimer was able to diffuse from the injection site while G4-C12 was completely blocked in place. Such a different behavior is probably due to the higher hydrophobicity of the C12 lipid chains and a feasible stronger interaction with the surrounding cell membranes and extracellular matrix (ECM) in comparison to the surface nature of G4. 70 kDa neutral dextran was used as a control. This linear and neutral macromolecule diffuses much faster than dendrimers in the ECM, and its fluorescence signal is completely faded away in less than 1 min. Our results demonstrated that the dendrimer surface properties drive their diffusion ability in vivo.

G4 and G4-C12 PAMAM Dendrimer Toxicity in Primary Cortical Neuron in Vitro and in Vivo. To evaluate PAMAM dendrimer toxicity on neurons we tested them in primary culture in vitro and after IP injection in vivo.

Primary neural cultures have been treated for 24 h in normal culturing conditions (culture medium, 37 °C, 5% CO_2) in the absence or presence of increasing G4 and G4-C12 PAMAM dendrimer concentrations, ranging from 1 to 100 nM. Figure 5A (left graph) shows the percentage of viable cells in culture after dendrimer administration. Viable cell number statistically decreases at 100 nM G4 and G4-C12 PAMAM dendrimer concentration. 24 h exposure at a concentration of 100 nM G4 PAMAM dendrimer reduces by 22% the viable primary neurons, while the presence of 100 nM G4-C12 in culture strongly diminishes (74%) their number. Most of the G4-C12 PAMAM dendrimer treated neurons die by apoptosis (51% of the total cell death) as shown in the right graph of Figure 2A, suggesting a crucial role of the C-12 lipid chain functionalization in the impairment of cell survival mechanisms of differentiated (post-mitotic) cortical cells. On the other hand, cell death of glia cells was not observed at the nM range of concentrations used in the described experiments (Figure 4 in the Supporting Information). Our results emphasized the apoptotic cell death induced by C-12 lipid chain modified dendrimer at low concentrations in primary neurons in vitro, prompting us to the following in vivo investigation.

IP injection in the mouse brain cortex of 1 μM PAMAM labeled dendrimers has been performed in order to verify their apoptotic effect in the brain in vivo (Figure 5B). Three days after the surgery, propidium iodide staining of mouse brain slices revealed the presence of damage close to G4-C12 PAMAM dendrimer injection site in the cortex. This damaged area (Figure 5Bd) was visibly wider when compared to that observed after both control (Figure 5Ba) and G4 injection (Figure 5Bg). Moreover, apoptotic detection with TUNEL assay showed the presence of programmed cell death reaction in the same sample (Figure 5Be), which is not activated in the presence of G4 PAMAM dendrimer (Figure 5Bh) nor in the absence of dendrimer (Figure 5Bb). Apoptotic cell signal spatially coincided with the G4-C12 PAMAM dendrimer accumulation in the parenchyma indicating that higher concentration of dendrimer could be toxic, in agreement with what we saw in culture (Figure 5Bf), while no G4 PAMAM accumulation was detected around the injection site where there is no sign of apoptosis (Figure 5Bi).

This information from in vivo experiments confirmed the in vitro data (Figure 5A), that is, the lower toxicity of G4 PAMAM dendrimers with respect to the higher level of apoptotic cell death induced by the same concentration of G4-C12 modified PAMAM. Furthermore, the presence of lipid-modified dendrimers in the site of injection (Figure 5Bf) implies the low diffusion rate of these nanoparticles. On the contrary, the absence of G4 PAMAM (Figure 5Bi) near the site of injection three days after dendrimer administration confirms their diffusion, as observed *ex vivo* by conventional confocal and in vivo 2-photon microscopy (Figure 2, Figure 3 and Figure 4).

In Vivo Two-Photon Calcium Imaging and Local Field Potential Electrophysiological Recordings in Mouse Visual Cortex Injected with G4-PAMAM. To evaluate viability and activity of neuron and astrocytes in the presence of amine-PAMAM dendrimer we performed in vivo two-photon calcium imaging and local field potential electrophysiological

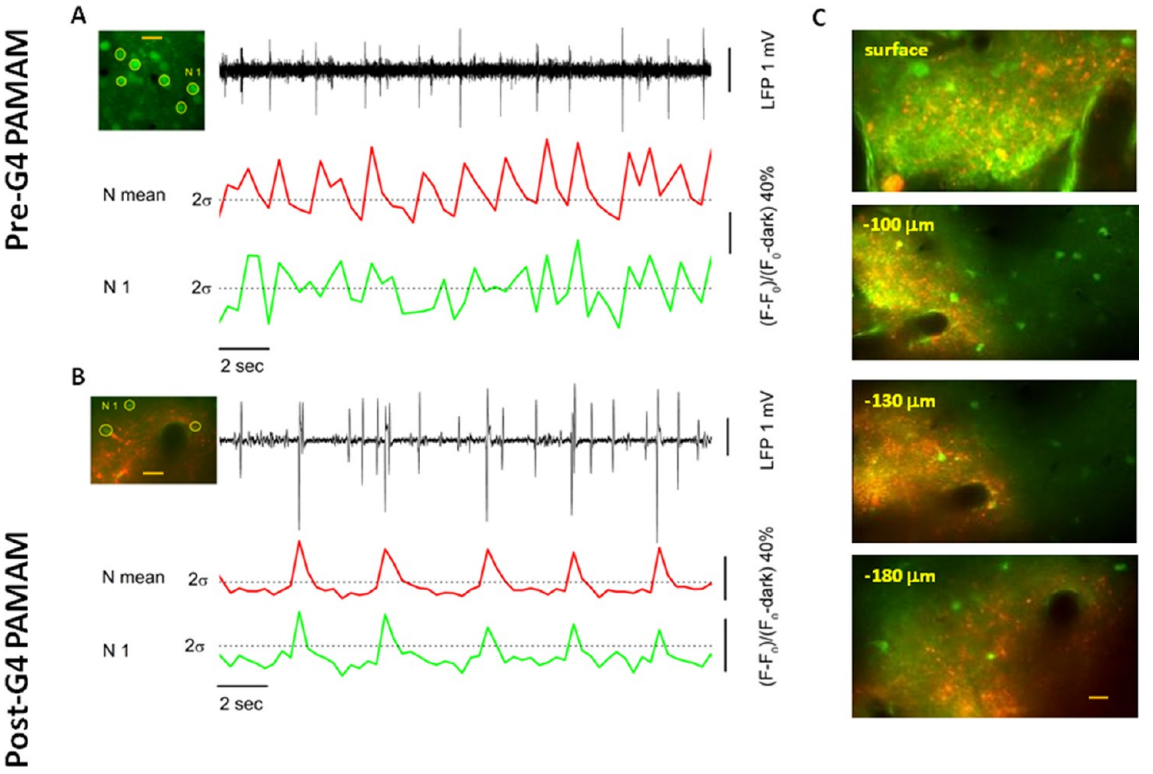

Figure 6. In vivo two-photon calcium imaging and local field potential electrophysiological recordings in mouse visual cortex injected with G4-Rhodamine labeled PAMAM. (A) Before G4-Rhod injection. Left panel: average projection of a two-photon imaging time series performed 150 mm deep in the visual cortex of anesthetized mouse locally loaded with calcium indicator OGB-1 AM before injection of G4-Rhod. The green signal is proportional to $[Ca^{2+}]_i$. Yellow circles highlight neuron somata. Calibration bar: 20 mm. Right panel: top trace is the LFP (t) recorded with extracellular electrode positioned in the proximity of the imaged field (approximately 50 mm, not shown). Red trace is the DF/F (t): fluctuation of green fluorescence intensity proportional to $[Ca^{2+}]_i$ relative to 6 neurons encircled in the left panel and normalized by the mean value of fluorescence in the 6 ROIs calculated across the whole time series. The green trace is the DF/F (t) of a single neuron (N1) from the same series. The dotted lines represent the 2 s threshold below which DF/F (t) falls in the noise regimen. (B) After G4-Rhod injection. Left panel is the average projection of a two-photon calcium imaging time series performed 150 mm deep in the visual cortex of the same anesthetized mouse in panel A, locally loaded with Calcium indicator OGB-1 AM 1 min after microinjection (0.5 psi) of G4-Rhod in ACSF (300 mM, 2 mL). The green signal is proportional to $[Ca^{2+}]_i$ while the red one originates from the fluorescent moiety of the injected G4-Rhod. Yellow circles highlight neuron somata. Calibration bar: 20 mm. Right panel: LFP trace presents the same synchronous activity depicted in panel A. Red and green traces indicate DF/F (t) as in panel A. Intense neural activity both at the cellular and population level is clearly visible. The difference in LFP and DF/F (t) magnitude between panels A and B is attributable to the neural synchronization degree that increases with time from the BMI superfusion. (C) Average time series projections acquired with two-photon imaging at different depths as indicated in yellow, performed 2 h after dendrimer microinjection. G4-Rhod localization appears stable within 5−10 min from the delivery till the end of the experiment (>2 h). Spatial distribution indicates an asymmetry toward neuropile structures, particularly astrocytic processes as estimated from exclusively morphological criteria.

recordings in mouse visual cortex injected with G4-Rhodamine labeled PAMAM. As represented in Figure 6, neurons are still responsive after pharmacological treatments in the presence or absence of injected G4-PAMAM dendrimer released in the surrounding environment. We trigged neural electrophysiological activity by superfusion with $GABA_AR$ antagonist bicuculline-methiodide at a concentration of 2 mM dropped on the meningeal dura surface 2 min before the acquisition. This pharmacological treatment increased the otherwise low rate of neural activity. Each deflection in LFP was generated by a synchronous firing of neuronal population. In our recorded data each calcium peak was mirrored by electrophysiological spikes, indicating ongoing single and population neural activity of "healthy" cells.

Our data demonstrate neural activity in the presence of G4 PAMAM dendrimers.

Astrocyte and Microglia Response to Dendrimer Injections. We have shown the effect of PAMAM dendrimers on neural cell death in vitro and in vivo. However cell death is not the only relevant aspect of brain toxicity. Indeed, we carried out an investigation of brain immune resident cell activation upon dendrimer administration (Figure 7). Mice were injected with G4 PAMAM, the dendrimer able to diffuse in the brain parenchyma, and lipopolysaccharide (LPS) respectively in the left and right brain hemispheres. LPS was used as an internal positive control to induce brain resident immune competent cell activation. PBS negative control intraparenchyma injection was also performed to evaluate the injection damage (Figure 5 in the Supporting Information). Low magnification images (Figure 7A) showed that both G4 and LPS visibly enhanced GFAP and IBA-1 expression in the injection site owing to the response to the tissue damage induced by the needle penetration in the tissue. However in the G4-injected hemisphere the activation was strictly localized in the injection site while for LPS a very broad area of inflammation can be observed. These results demonstrate the low glia activation due to the presence of G4 dendrimers, albeit its diffusion in a broad area of the parenchyma. Figure 7B shows representative high magnification confocal images of brain slices

dx.doi.org/10.1021/mp300391v | Mol. Pharmaceutics XXXX, XXX, XXX−XXX

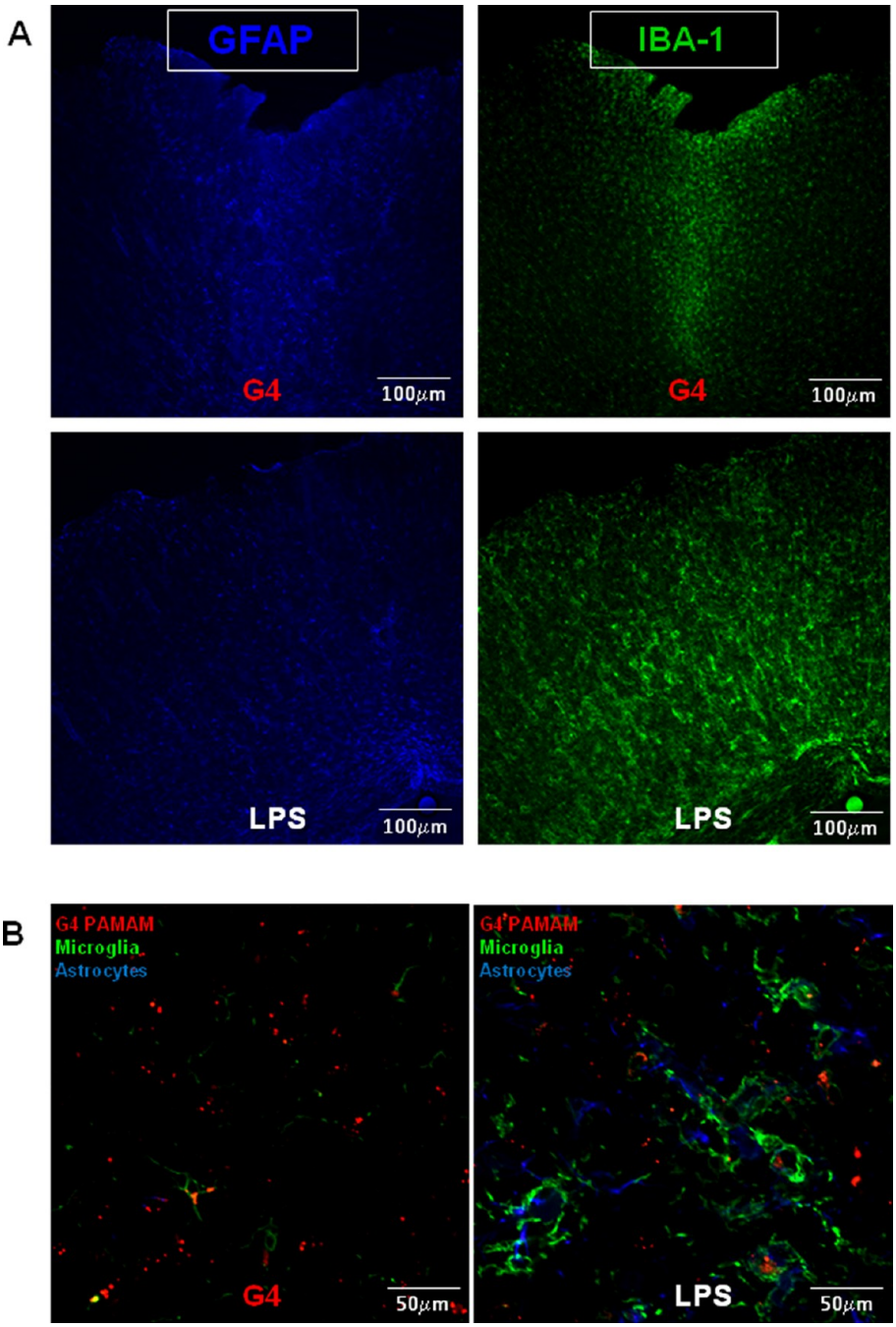

Figure 7. Brain resident immune cell activation. (A) Brain slices GFAP (blue) and IBA-1 (green) immunostained and imaged at the confocal microscope 10 days after G4 PAMAM and LPS intraparenchyma injections. (B) Triple staining of dendrimers (red), GFAP (blue) and IBA-1 (green). Mice were coinjected with Alexa 647 labeled dendrimers (left hemisphere, left panel) and LPS (right hemisphere, right panel).

from each hemisphere injected either with G4 or LPS. A triple staining was performed: (i) G4 dendrimers were labeled with the infrared dye Alexa 647 (showed in red); (ii) the activated astrocyte marker protein GFAP was visualized by Alexa 488 (shown in blue) and (iii) the activated microglia protein IBA-1 was labeled with Alexa 563 (showed in green). Notably dendrimers (red channel) are also present in the hemisphere injected with LPS demonstrating the remarkable diffusion ability of the G4 dendritic polymer (right panel). However, the higher microglia and astrocyte positive signals are very likely to be due to the presence of the LPS. Indeed, the very low fluorescence signal level in the green and blue channel (left panel) suggests the low level of glia activation even where high accumulation of dendrimer (red channel) is present.

According to previous reports,[17,18] we here demonstrate that activated glial cells have strong internalization ability for dendrimers as indicated by the bright green/red fluorescence signal colocalization.

DISCUSSION

A wide literature about PAMAM dendrimers' interaction with different types of cells is available today. Nevertheless, the majority of the experimental results is obtained with cell lines and

dx.doi.org/10.1021/mp300391v | *Mol. Pharmaceutics* XXXX, XXX, XXX−XXX

very little information is available about their effects on primary neurons in vivo.

Owing to their slow membrane recycling and downregulated metabolism, neurons are a difficult target for nanocarrier-driven delivery that relies on endocytosis. Notably, the possibility of local accumulation in intracellular acidic vesicles, as shown by our results, is of particular importance in light of the design of pH-responsive delivery vectors or to generate selective drug delivery systems for high incidence metabolic disorders such as lysosomal storage disease.[19]

Our results of G4 PAMAM penetration ability into brain parenchyma crossing the ependymal barrier after intracerebroventricular administration demonstrate its potential in view of future nanodelivery systems. Remarkably, the ICV method allows soluble drugs to reach a different part of the CNS, connected by the ventricular space, bypassing the BBB.[20] This delivery method, already in use for therapies aimed at CNS such as the delivery of antibiotic for CNS infections or antiepileptic agents, reduces the drug dose and its possible side effects, protecting the drug molecule from enzymatic interference and increasing its efficacy. However, drugs that are injected into the cerebrospinal fluid (CFS) compartment should be rapidly transported out of the brain to the blood and their entry into the parenchyma slower than CSF convection and bulk flow.[21] Our results demonstrate that G4 PAMAM dendrimer diffusion into the brain parenchyma is sufficiently fast to find them in all the different layers of the neural tissue. To reinforce our data, in view of long-term therapies,[22] we also delivered G4 PAMAM dendrimers to the CSF compartment through the subarachnoid space. As well as other authors,[23,24] we observed diffusion and cell internalization confirming the potential for PAMAM dendrimer mediated drug delivery through the brain tissue from the CSF regardless of the administration site of injection. We clearly showed a marked difference in the diffusion pattern and toxicity between two different nanoparticle surface modifications. We proved that the lipophilic nature of G4-C12 prevents dendrimer from moving deeper into the parenchyma.

Cationic PAMAMs have been reported to be toxic for several cell lines and primary blood cells.[25] PAMAM dendrimer toxicity increases with surface change (e.g., G6 more toxic then G4) and structure related mechanistic studies have revealed ROS production, lysosomal activity, DNA damage and apoptosis.[26,27] However, all these reported results indicate G4 PAMAM induced toxicity in vitro at micromolar concentrations. We found low toxicity at nanomolar concentrations of cationic G4 PAMAM in our in vitro experiments with primary neurons. For the sake of accuracy, it has to be noted that noxious effects in the nanomolar concentration range of dendrimers have been revealed in cell lines by clonogenic assay, nevertheless, this test is not applicable to postmitotic primary neurons. Differently from the cationic surface of the dendrimer, the C12 lipid moieties evidently induce apoptotic cell death of primary neurons even at nanomolar concentrations. Programmed cell death induced by nanomolar concentrations of C12-G4 dendrimer might be specific for finally differentiated cells, like primary neurons. This observation does not exclude the possibility to observe cell apoptosis induced by amine-G4 at higher concentration, although necrosis is the suggested main mechanism of cell death induced by G4 PAMAM dendrimer in the micromolar range in vitro.[26,27]

Immune competent cells of the CNS are moderately activated in vivo by the presence of G4 PAMAM dendrimers. This activation is limited to the site of injection, suggesting a role of the invasive procedure of administration as the first responsible for the observed glia activation. However, more focused studies on the microglia activation and inflammatory reaction induced by PAMAM dendrimers will be needed in the future to define a precise risk assessment for their use in clinical applications.

In this work we explored the behavior of different PAMAM dendrimers in the CNS. Particular emphasis was put on dendrimer dynamic localization and toxicity, two very important issues for therapeutic use of nanocarriers. We demonstrate that G4 PAMAM dendrimer is endowed with many desirable properties for delivery applications such as low toxicity, low immune response, and high tissue diffusion ability. Moreover, we demonstrated that G4 dendrimers are taken up by neuronal cells in vivo with increased internalization only in preactivated microglia. We believe this work reveals crucial insights into PAMAM behavior in the CNS and opens G4 PAMAM application as a nanomaterial for in vivo delivery in the CNS.

■ ASSOCIATED CONTENT

Ⓢ Supporting Information

Additional figures depicting G4-C12 PAMAM internalization in primary neurons, Hoechst stained coronal slice of entire mouse brain, subarachnoid injection, G4 and G4-C12 PAMAM dendrimer toxicity in primary cortical glia in vitro, and PBS injection as negative control for GFAP/IBA-1 staining. Table of dendrimer *Z* potentials. This material is available free of charge via the Internet at http://pubs.acs.org.

■ AUTHOR INFORMATION

Corresponding Author

*G.B.: Center for Nanotechnology Innovation @NEST, Istituto Italiano di Tecnologia Piazza San Silvestro 12, 56127 Pisa, Italy; phone, +39 050 509736; fax, +39 050 509417; e-mail, giuseppe.bardi@iit.it. L.A.: Eindhoven University of Technology, Den Dolech 2, 5612AZ Eindhoven, The Netherlands; phone, +310402473912; e-mail, L.Albertazzi@tue.nl.

Notes

The authors declare no competing financial interest.

■ ACKNOWLEDGMENTS

We thank Alice Bertero, Alberto Galbusera and Adriano Boni for their technical assistance. The activity presented in this work has been supported by Fondazione Istituto Italiano di Tecnologia.

■ REFERENCES

(1) Lee, C. C.; Gillies, E. R.; Fox, M. E.; Guillaudeu, S. J.; Frechet, J. M.; Dy, E. E.; Szoka, F. C. A single dose of doxorubicin-functionalized bow-tie dendrimer cures mice bearing C-26 colon carcinomas. *Proc. Natl. Acad. Sci. U.S.A.* **2006**, *103* (45), 16649−54.

(2) Baker, J. R., Jr. Dendrimer-based nanoparticles for cancer therapy. *Hematology* **2009**, 708−19.

(3) Yellepeddi, V. K.; Kumar, A.; Palakurthi, S. Surface modified poly(amido)amine dendrimers as diverse nanomolecules for biomedical applications. *Expert Opin. Drug Delivery* **2009**, *6* (8), 835−50.

(4) Tomalia, D. A.; Huang, B.; Swanson, D. R.; Brothers, H. M.; Klimash, J. W. Structure control within poly(amidoamine) dendrimers: size, shape and regio-chemical mimicry of globular proteins. *Tetrahedron* **2003**, *59* (22), 3799−813.

(5) Jensen, L. B.; Pavan, G. M.; Kasimova, M. R.; Rutherford, S.; Danani, A.; Nielsen, H. M.; Foged, C. Elucidating the molecular mechanism of PAMAM-siRNA dendriplex self-assembly: effect of dendrimer charge density. *Int. J. Pharm.* **2011**, *416* (2), 410−8.

(6) Perumal, O. P.; Inapagolla, R.; Kannan, S.; Kannan, R. M. The effect of surface functionality on cellular trafficking of dendrimers. *Biomaterials* **2008**, *29* (24−25), 3469−76.

(7) Xu, Q.; Wang, C. H.; Pack, D. W. Polymeric carriers for gene delivery: chitosan and poly(amidoamine) dendrimers. *Curr. Pharm. Des.* **2010**, *16* (21), 2350−68.
(8) Duncan, R.; Izzo, L. Dendrimer biocompatibility and toxicity. *Adv. Drug Delivery Rev.* **2005**, *57* (15), 2215−37.
(9) Costantino, L. Drug delivery to the CNS and polymeric nanoparticulate carriers. *Future Med. Chem.* **2010**, *2* (11), 1681−701.
(10) Al-Jamal, K. T.; Gherardini, L.; Bardi, G.; Nunes, A.; Guo, C.; Bussy, C.; Herrero, M. A.; Bianco, A.; Prato, M.; Kostarelos, K.; Pizzorusso, T. Functional motor recovery from brain ischemic insult by carbon nanotube-mediated siRNA silencing. *Proc. Natl. Acad. Sci. U.S.A.* **2011**, *108* (27), 10952−7.
(11) Kalladka, D.; Muir, K. W. Stem cell therapy in stroke: designing clinical trials. *Neurochem. Int.* **2011**, *59* (3), 367−70.
(12) Karussis, D.; Karageorgiou, C.; Vaknin-Dembinsky, A.; Gowda-Kurkalli, B.; Gomori, J. M.; Kassis, I.; Bulte, J. W.; Petrou, P.; Ben-Hur, T.; Abramsky, O.; Slavin, S. Safety and immunological effects of mesenchymal stem cell transplantation in patients with multiple sclerosis and amyotrophic lateral sclerosis. *Arch. Neurol.* **2010**, *67* (10), 1187−94.
(13) Vender, J.; Waller, J.; Dhandapani, K.; McDonnell, D. An evaluation and comparison of intraventricular, intraparenchymal, and fluid-coupled techniques for intracranial pressure monitoring in patients with severe traumatic brain injury. *J. Clin. Monit. Comput.* **2011**, *25* (4), 231−6.
(14) Albertazzi, L.; Serresi, M.; Albanese, A.; Beltram, F. Dendrimer internalization and intracellular trafficking in living cells. *Mol. Pharmaceutics* **2010**, *7* (3), 680−8.
(15) Bardi, G.; Malvindi, M. A.; Gherardini, L.; Costa, M.; Pompa, P. P.; Cingolani, R.; Pizzorusso, T. The biocompatibility of amino functionalized CdSe/ZnS quantum-dot-Doped SiO2 nanoparticles with primary neural cells and their gene carrying performance. *Biomaterials* **2010**, *31* (25), 6555−66.
(16) Mandell, J. G.; Neuberger, T.; Drapaca, C. S.; Webb, A. G.; Schiff, S. J. The dynamics of brain and cerebrospinal fluid growth in normal versus hydrocephalic mice. *J. Neurosurg. Pediatr.* **2010**, *6* (1), 1−10.
(17) Iezzi, R.; Guru, B. R.; Glybina, I. V.; Mishra, M. K.; Kennedy, A.; Kannan, R. M. Dendrimer-based targeted intravitreal therapy for sustained attenuation of neuroinflammation in retinal degeneration. *Biomaterials* **2012**, *33* (3), 979−88.
(18) Wang, B.; Navath, R. S.; Romero, R.; Kannan, S.; Kannan, R. Anti-inflammatory and anti-oxidant activity of anionic dendrimer-N-acetyl cysteine conjugates in activated microglial cells. *Int. J. Pharm.* **2009**, *377* (1−2), 159−68.
(19) Beck, M. Therapy for lysosomal storage disorders. *IUBMB Life* **2010**, *62* (1), 33−40.
(20) Barcia, J. A.; Gallego, J. M. Intraventricular and intracerebral delivery of anti-epileptic drugs in the kindling model. *Neurotherapeutics* **2009**, *6* (2), 337−43.
(21) Pardridge, W. M. Drug transport in brain via the cerebrospinal fluid. *Fluids Barriers CNS* **2011**, *8* (1), 7−10.
(22) Ghafoor, V. L.; Epshteyn, M.; Carlson, G. H.; Terhaar, D. M.; Charry, O.; Phelps, P. K. Intrathecal drug therapy for long-term pain management. *Am. J. Health-Syst. Pharm.* **2007**, *64* (23), 2447−61.
(23) Dai, H.; Navath, R. S.; Balakrishnan, B.; Guru, B. R.; Mishra, M. K.; Romero, R.; Kannan, R. M.; Kannan, S. Intrinsic targeting of inflammatory cells in the brain by polyamidoamine dendrimers upon subarachnoid administration. *Nanomedicine (London)* **2010**, *5* (9), 1317−29.
(24) Wang, B.; Navath, R. S.; Menjoge, A. R.; Balakrishnan, B.; Bellair, R.; Dai, H.; Romero, R.; Kannan, S.; Kannan, R. M. Inhibition of bacterial growth and intramniotic infection in a guinea pig model of chorioamnionitis using PAMAM dendrimers. *Int. J. Pharm.* **2010**, *395* (1−2), 298−308.
(25) Feliu, N.; Walter, M. V.; Montanez, M. I.; Kunzmann, A.; Hult, A.; Nystrom, A.; Malkoch, M.; Fadeel, B. Stability and biocompatibility of a library of polyester dendrimers in comparison to polyamidoamine dendrimers. *Biomaterials* **2012**, *33* (7), 1970−81.
(26) Mukherjee, S. P.; Davoren, M.; Byrne, H. J. In vitro mammalian cytotoxicological study of PAMAM dendrimers - towards quantitative structure activity relationships. *Toxicol In Vitro* **2010**, *24* (1), 169−77.
(27) Mukherjee, S. P.; Lyng, F. M.; Garcia, A.; Davoren, M.; Byrne, H. J. Mechanistic studies of in vitro cytotoxicity of poly(amidoamine) dendrimers in mammalian cells. *Toxicol. Appl. Pharmacol.* **2010**, *248* (3), 259−68.

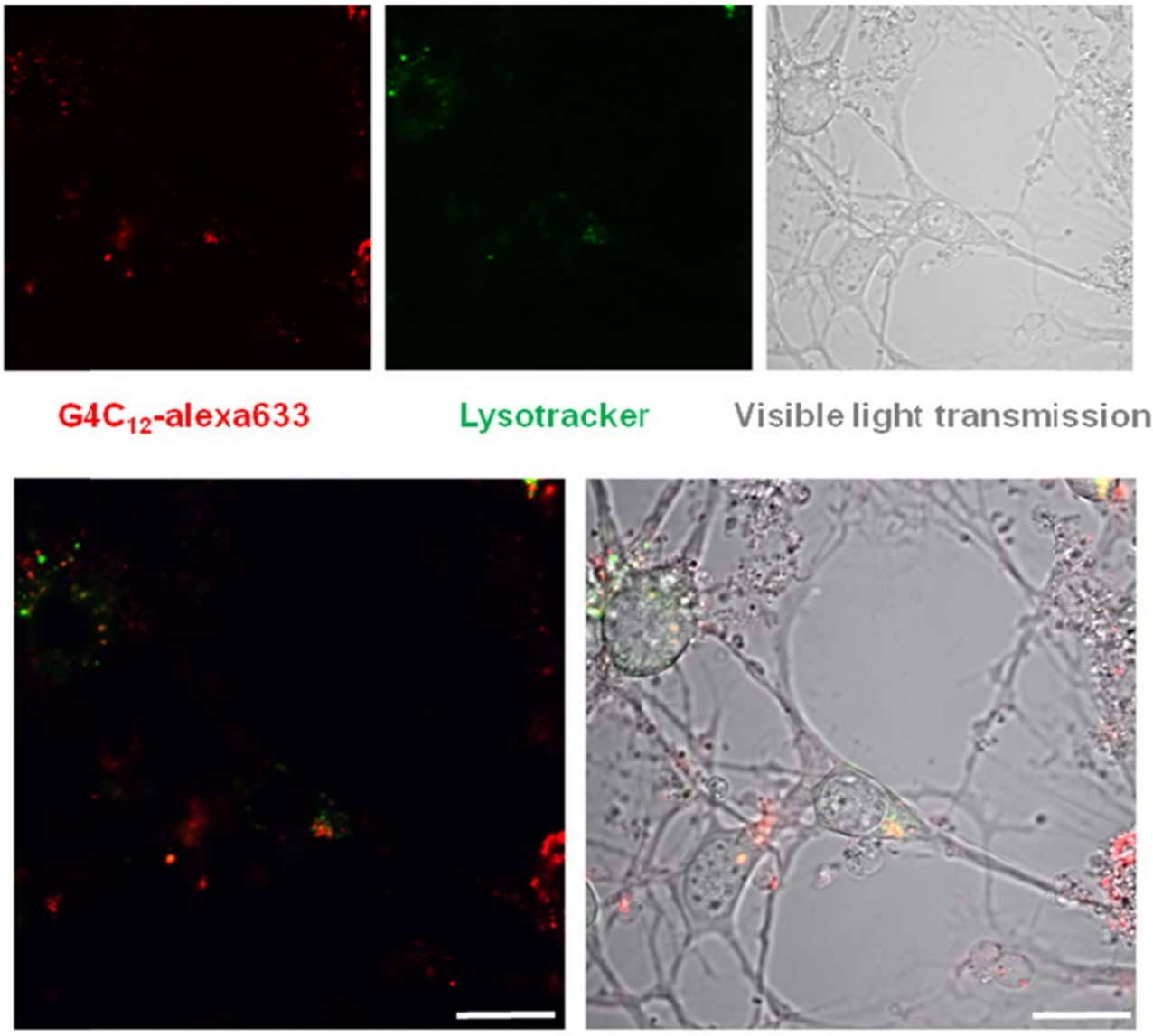

Supporting Information Figure 1 G4-C_{12} PAMAM internalization in primary neurons.
Intracellular localization of G4-C_{12} in primary neuronal cultures. Pictures were obtained 4h after 10nM PAMAM administration. (AF647 labeled dendrimer, Red; lysotracker, green). Scale bar = 10µm.

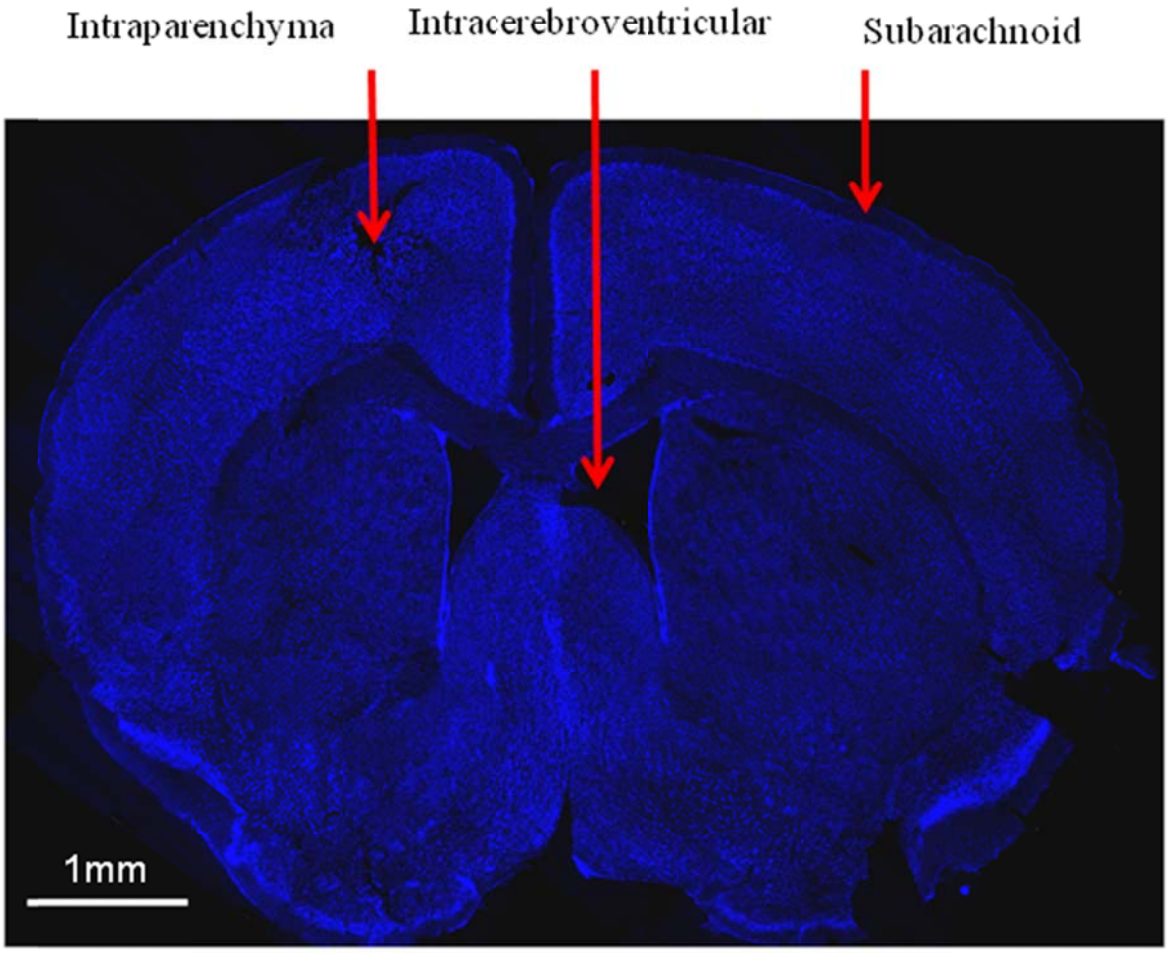

Supporting Information Fig 2 Dendrimer administration methods

Hoechst stained coronal slice of entire mouse brain. Red arrows indicate the way of dendrimer administration.

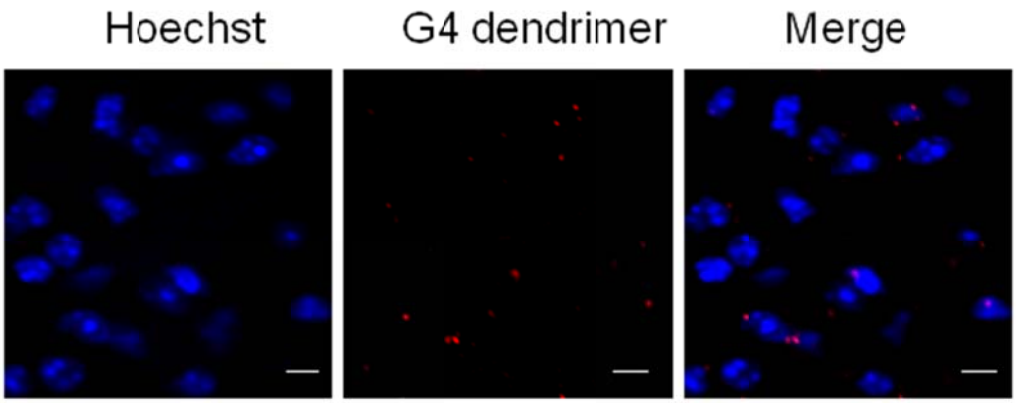

Supporting Information Fig 3 Subarachnoid injection.

Dendrimer (red) cell uptake following subarachnoid injection. Nuclei were stained with hoechst. Dendrimers showed the characteristic perinuclear localization typical of endocytosis. Scale bar = 10μm.

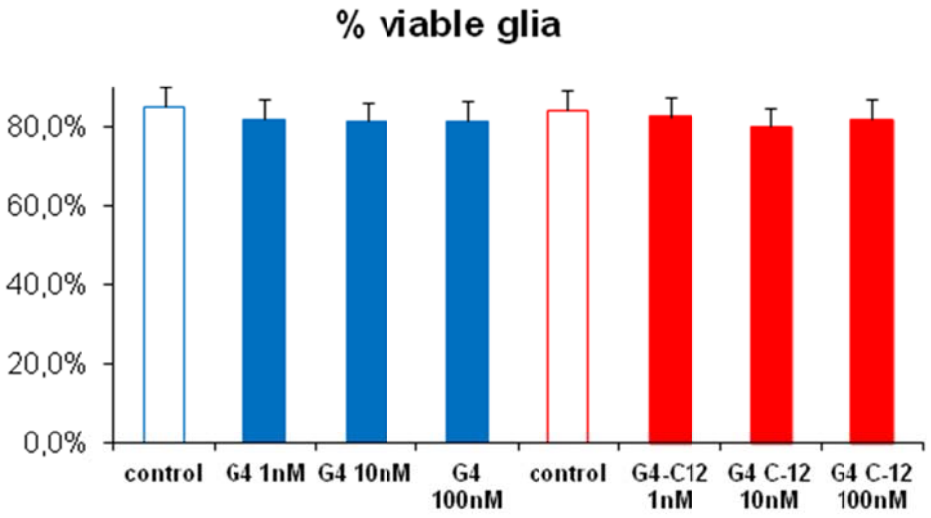

Supporting Information Fig 4 G4 and G4-C12 PAMAM dendrimer toxicity in primary cortical glia *in vitro*

Viable glia were counted 24 hours after treatment with increasing concentration of G4 and G4-C12 PAMAM dendrimers and the results expressed in percentage of cells after treatments compared to control (untreated). The data are expressed as mean ± SEM of three independent experiments.

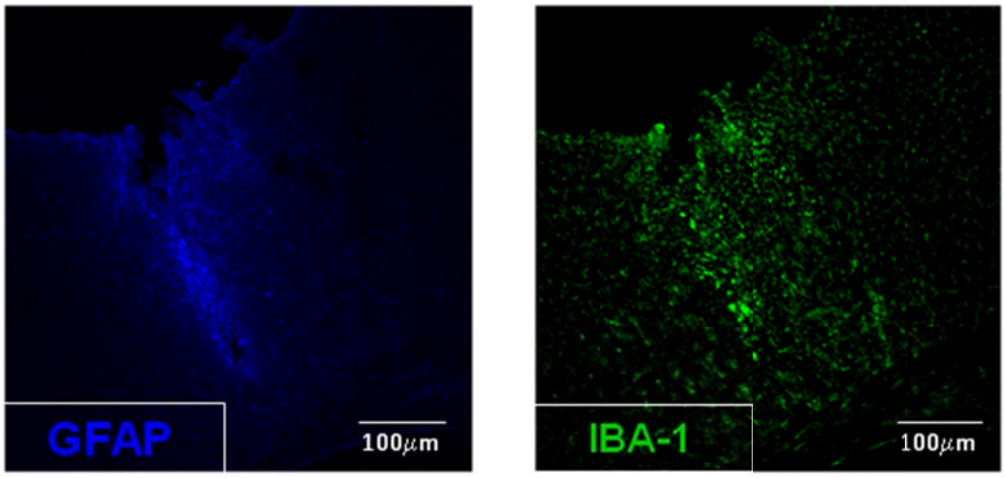

Supporting Information Figure 5 PBS injection as negative control for GFAP/IBA-1 staining.

A) brain slices GFAP (blue) and IBA-1 (green) immunostained and imaged at the confocal microscope 10 days after LPS intraparenchyma injections.

Dendrimer	Hydrodynamic mean diameter (nm)	Z-potential (mV)
PAMAM G4	3.9	+9.0
PAMAM-C_{12} G4	4.0	+5.8

Supporting Information Table 1 Dendrimer Z-potentials

Dynamic Light Scattering (DLS) measurements were performed on a Zetasizer ZS90 instrument (size diameter detection from 0.3nm to 5 microns) using 90 degree scattering optics (Malvern Instruments Ltd).